

Evidence for Black Holes in Green Peas from *WISE* colors and variability

SANTOSH HARISH,¹ SANGEETA MALHOTRA,^{2,1} JAMES E. RHOADS,^{2,1} TIANXING JIANG,¹ HUAN YANG,³ AND KENDRICK KNORR¹

¹*School of Earth and Space Exploration, Arizona State University, Tempe, AZ 85287, USA*

²*NASA Goddard Space Flight Center, 8800 Greenbelt Road, Greenbelt, MD 20771, USA*

³*Las Campanas Observatory, Carnegie Institution for Science, Chile*

ABSTRACT

We explore the presence of active galactic nuclei (AGN)/black hole (BH) in Green Pea galaxies (GPs), motivated by the presence of high ionization emission lines such as HeII and [NeIII] in their optical spectra. In order to identify AGN candidates, we used mid-infrared (MIR) photometric observations from the all-sky Wide-field Infrared Survey Explorer (*WISE*) mission for a sample of 516 GPs. We select 58 GPs as candidate AGN based on a stringent 3-band *WISE* color diagnostic. Using multi-epoch photometry of *W1* and *W2* bands from the *WISE/NEOWISE-R* observations, we find 38 GPs showing significant variability in both the *WISE* bands. Four of these were selected as AGN by the *WISE* 3-band color diagnostic as well. Interestingly, we find a high fraction of MIR variable sources among GPs which demonstrates the uniqueness and importance of studying these extreme objects. Through this work, we demonstrate that photometric variability is a promising tool to select AGN that may be missed by other selection techniques (including optical emission-line ratios and X-ray emission) in star-formation dominated, low-mass, low-metallicity galaxies.

Keywords: galaxies: dwarf – galaxies: starburst – galaxies: nuclei – galaxies: evolution

1. INTRODUCTION

Since their discovery more than a decade ago, *Green Peas* (GPs; Cardamone et al. 2009), a class of low-redshift ($z \lesssim 0.3$) extreme emission-line galaxies, have been studied extensively across the entire electromagnetic spectrum. These galaxies exhibit intense star formation activity, strong nebular lines, low metallicity, low dust content and high gas pressures (e.g., Izotov et al. 2011; Yang et al. 2016, 2017a; Jiang et al. 2019; Kim et al. 2020). They are also compact in size (Kim et al. 2021) and typically contain low stellar mass. UV studies of Green Peas have shown the prevalence of Ly α emission-line with an equivalent width distribution matching those of high-redshift ($z \sim 3 - 6$) Ly α emitters (e.g., Henry et al. 2015; Yang et al. 2016, 2017b). They exhibit high [OIII]/[OII] ratios, which are seen in some high- z galaxies, and which may indicate the presence of optically thin ionized regions (e.g., Jaskot & Oey 2013; Nakajima & Ouchi 2014). And, there is growing evidence that Lyman continuum radiation escapes

more readily in Green Peas (with escape fractions 2-72%; Izotov et al. 2016; Yang et al. 2017b; Izotov et al. 2018) than in any other known galaxy population, making them the best available low- z analogs of the galaxies that drove cosmological reionization. GPs are selected on the basis of optical emission lines (generally [OIII]) with extreme equivalent widths. They often exhibit high ionization nebular lines such as HeII 4686Å and [NeIII] 3869Å, which suggest a hard ionizing source such as active galactic nuclei (AGN). However, the relative importance of star formation and accretion in powering GP activity remains poorly known.

Over the last few decades, there is a growing consensus that most massive galaxies host super-massive black holes (SMBHs) in their central regions (Kormendy & Richstone 1995; Kormendy & Ho 2013). Less is known about black holes (BHs) among low-mass galaxies, although there has been an increase in low-mass BH candidates in the recent times (e.g., Greene & Ho 2007; Reines et al. 2013). Low-mass galaxies can be crucial in placing constraints on models of BH seed formation and non-merger models of BH evolution (e.g., Volonteri & Natarajan 2009; van Wassenhove et al. 2010; Greene 2012). Detection of AGN signatures in low-mass galax-

ies is a significant challenge. A large fraction of these AGNs may be missed by optical selection either because the central engine is obscured, or because emission-line indicators such as [OIII] are contaminated by extreme star formation in the host galaxy (e.g., Gouling & Alexander 2009; Trump et al. 2015). With X-ray selection, the presence of high-mass X-ray binaries (HMXBs) and ultra-luminous X-ray sources (ULXs) pose a serious challenge in the detection of low-mass BHs because of their comparable luminosities (e.g., Lehmer et al. 2010; Mineo et al. 2012).

Mid-infrared (MIR) AGN selection has shown promise in identifying some obscured, optically hidden AGN in several galaxies. The hard radiation field produced by the AGN can heat dust to high temperatures, generating strong MIR continuum and an infrared SED that is distinct from typical star-forming galaxies. The AGN continuum emission is approximately a power law in the $3 - 10\mu\text{m}$ range, because strong UV and X-ray radiation destroys the molecules responsible for the Polycyclic Aromatic Hydrocarbon (PAH) emission, while heating the surrounding grains to near dust sublimation temperatures ($1000 - 1500\text{K}$). With the advent of Wide-field Infrared Survey Explorer (*WISE*), a large number of AGN have been identified, demonstrating that MIR color diagnostics can select luminous AGN with a 95% reliability (e.g., Stern et al. 2012)

An alternate way to identify AGN is based on flux variability. Active nuclei are known to be variable in different spectral regimes with timescales ranging from hours to years (e.g., Sesar et al. 2007; Kozłowski et al. 2016). The variability is thought to be related to thermal fluctuations in the accretion disk driven by a turbulent magnetic field (Kelly et al. 2009) and/or temperature fluctuations in an inhomogenous accretion disk (Ruan et al. 2014). Variability-based selection is a promising means for finding massive BHs in dwarf galaxies. Several studies in the past have shown that such a selection can (1) identify AGN in the low-mass, low-metallicity regime missed by other selection techniques (e.g., Baldassare et al. 2018), (2) identify low-luminosity AGN (Trevese et al. 1994), and (3) identify AGN in dwarf galaxies where host galaxy emission dominates the total luminosity (e.g., Trump et al. 2015).

In this paper, we present findings from the first-ever systematic search for AGN in GPs using MIR observations. Section 2 describes the GP sample and the relevant MIR *WISE* photometric data. The MIR color and variability diagnostic used for AGN selection is presented in Section 3. The results and comparison with other selection methods are discussed in Section 4. Our main conclusions are presented in Section 5. All magni-

tudes presented in this work are in Vega system, unless stated otherwise.

2. SAMPLE AND DATA

The sample of Green Pea galaxies were selected following Jiang et al. (2019). In total, there are 1004 objects that are spatially compact ($R_{90} < 3''$), which contain well-detected ($\text{SNR} > 5$), strong [OIII] $_{\lambda 5007}$ and/or $H\beta$ emission-lines ($\text{EW}([\text{OIII}]_{\lambda 5007}) > 300\text{\AA}$ and/or $\text{EW}(H\beta) > 100\text{\AA}$), and have a literature spectral classification of ‘‘Galaxy’’ with a sub-class of ‘‘starforming,’’ ‘‘starburst,’’ or ‘‘NULL.’’ The literature classifications are drawn from the *galSpecLine* (Brinchmann et al. 2004; Tremonti et al. 2004) and *emissionLines-Port* (Maraston et al. 2013; Thomas et al. 2013) catalogs, based on SDSS Data Release 8 (Aihara et al. 2011) and 12 (Alam et al. 2015), respectively. The object classification is based on the measured optical emission-line ratios. However, as discussed in Section 4.1, some of these sources might still contain an AGN that is indistinguishable from a star-forming object based on optical spectroscopy alone.

2.1. WISE MIR data

The WISE mission (Wright et al. 2010) conducted a mid-infrared imaging survey of the entire sky using 3.4, 4.6, 12, and 22 μm bandpasses (hereafter, $W1$, $W2$, $W3$ and $W4$), in 2010. With a field-of-view of $47' \times 47'$ and angular resolution of $\sim 6''$ ($W1$, $W2$, $W3$) and $\sim 12''$ ($W4$), WISE scanned the entire sky once every six months with 12 or more independent, single-exposures of each point on the sky. The WISE solid hydrogen cryogen was exhausted in late 2010, and the spacecraft was put into hibernation in February 2011 after surveying the full sky twice. The NEOWISE-R Post-Cryo mission (Mainzer et al. 2011) reactivated the spacecraft and has been surveying the sky from December 2013 to the present using the two bluer bandpasses, $W1$ and $W2$ (which remain usable after cryogen exhaustion).

The AllWISE Source Catalog contains the most reliable and accurate MIR photometry for over 747 million objects on the sky based on observations from the WISE cryogenic and NEOWISE post-cryo phases of the mission. This catalog is derived from the AllWISE Atlas intensity images ($1.37''/\text{pixel}$) which consists of co-added 7.7s $W1$ and $W2$ single-exposure images from the 4-Band, 3-Band cryogenic and post-cryo mission phases, and co-added 8.8s $W3$ and $W4$ single-exposure images from the 4-Band mission phase. In order to look for the MIR counterparts of GPs, we cross-matched them, based on their SDSS coordinates, with the AllWISE Source Catalog using a search radius of $2''$, and found matches for 516 GPs from our sample.

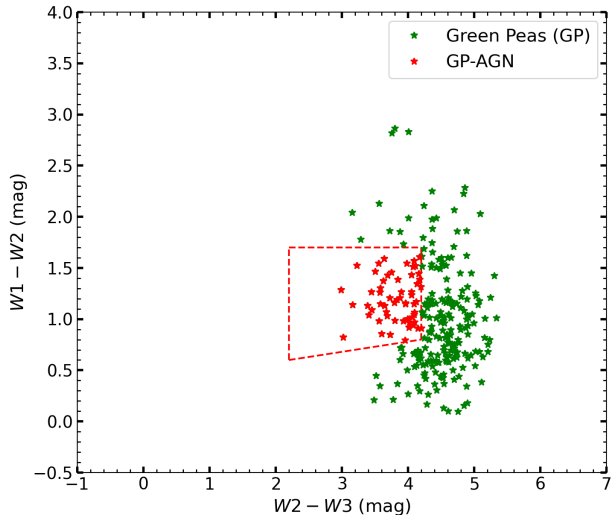


Figure 1. WISE color-color diagram for Green Peas. AGN candidates selected by the Jarrett et al. (2011) criteria are shown as red diamonds.

The WISE archives also contain time-tagged photometric measurements for source detections made on the individual 7.7s $W1$ and $W2$ single-exposure images from both WISE and NEOWISE-R mission phases; this should contain observations starting from 2010 until present, with a three-year gap between 2011 and 2014 when WISE was in hibernation. Typically, for most high SNR sources, there should be observations for at least 12 different epochs with multiple exposures ($\sim 10 - 20$) within each epoch. In order to construct the MIR light curves, we cross-matched our candidate GPs with two different single-exposure databases: (1) AllWISE Multiepoch Photometry database, which covers observations from 2010 to 2011, and (2) NEOWISE-R Single-Exposure Source database, which covers observations from 2014 till 2019, and gathered single-epoch, profile-fit photometry measurements in $W1$ and $W2$ bands. Care was taken to ensure that only good quality detections from good quality images were considered to construct the light curves, based on the guidelines provided in the Explanatory Supplement to the WISE¹ and NEOWISE² data products.

3. AGN SELECTION

3.1. WISE MIR colors

Several MIR color diagnostics exist in literature for selecting AGN, which are mostly based on data from either *Spitzer* (e.g., Stern et al. 2005; Lacy et al. 2007;

Donley et al. 2012) or *WISE* (e.g., Jarrett et al. 2011; Stern et al. 2012; Mateos et al. 2012). Since we are dealing with observations from *WISE*, we required our selection criteria to be defined based on *WISE* data that utilizes either one- or two-color criteria to select AGN. The one-color ($W1 - W2$) criterion, however, suffers from contamination from star-forming galaxies (e.g., Hainline et al. 2016). Therefore, we employed the more stringent two-color criteria by Jarrett et al. (2011) to select AGN candidates from our GP sample. As mentioned in Section 2.1, WISE photometry was available for 516 GPs in the AllWISE Source Catalog; however, considering only sources with $\text{SNR} \geq 5$ in $W1$, $W2$, and $W3$ bands, only 266 GPs were used for AGN selection based on MIR colors.

The $W3$ bandpass is sensitive to PAH ($11.3\mu\text{m}$) emission from nearby galaxies and shorter wavelength PAH (6.2 and $7.7\mu\text{m}$) emission from redshifted galaxies, as well as warm continuum from AGN at both low and high redshift. A typical “AGN” region in the MIR color space, encompassing QSOs and Seyfert galaxies, defined by Jarrett et al. (2011) is as follows:

$$2.2 < [W2 - W3] < 4.2, \text{ and} \quad (1) \\ (0.1 \times [W2 - W3] + 0.38) < [W1 - W2] < 1.7$$

58 GPs ($\sim 6\%$) were selected as AGN using these criteria. Figure 1 shows the location of GPs in the *WISE* color-color space and the selected AGN candidates based on this criteria. We note that this selection will mostly include AGN that are significant brighter than host galaxy emission. For weaker AGN, whose continuum emission is diluted by the host galaxy emission, their ($W1 - W2$) color can get bluer such that they become inseparable from normal star-forming galaxies (Stern et al. 2012).

3.2. WISE MIR variability

In order to select variable sources, we used multi-epoch WISE observations of GP objects in $W1$ and $W2$ bands, obtained over a period of ~ 9 years, as mentioned in Section 2. Given WISE’s scanning pattern, the single-exposure photometry in $W1$ and $W2$ is strongly clustered in time, with a cadence of 90 mins (in some cases, two exposures were taken 11s apart). In a single epoch, the number of observations varies significantly depending on the ecliptic latitude. Compared to optical variability arising from the accretion disk emission of an AGN, the MIR variability due to emission from the hot dust torus is expected to be smoothed out at shorter timescales because IR variations originate from a much bigger region than the optical variations (Kozłowski et al. 2016). Therefore, in this work,

¹ <http://wise2.ipac.caltech.edu/docs/release/neowise/expsup/sec2.3.html>

² <http://wise2.ipac.caltech.edu/docs/release/allwise/expsup/sec3.2.html>

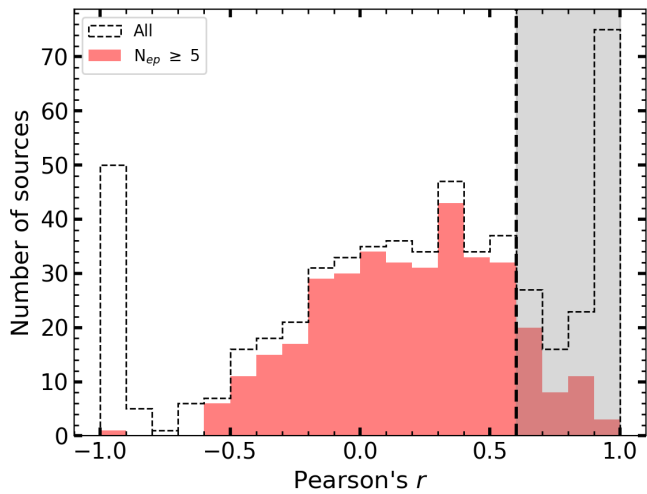


Figure 2. Distribution of Pearson correlation coefficient (r) of $W1$ and $W2$ for the full GP sample (*black histogram*) and GPs with observations in at least 5 epochs (*red histogram*). The *grey* shaded region denotes the sources with high correlation which are considered for variability selection along with other criteria, as mentioned in Section 3.2.

we concentrate on exploring the long-term variability of the GP sample. For this reason, we binned photometric measurements (in $W1$ and $W2$) within a 30-day window into individual epochs and quantified variability between these epochs, which are typically separated by ~ 6 months. Following Ai et al. 2010 and Kozłowski et al. 2010, we employed the amplitude of variability (σ_m) and Pearson correlation coefficient (r_{12}) metrics, based on photometry from $W1$ and $W2$, to select variable candidates among GPs. For sources in the sample with multi-epoch measurements, we calculated Pearson's r_{12} as

$$r_{12} = \frac{C_{12}}{\Sigma_{W1}\Sigma_{W2}} \quad (2)$$

where C_{12} is the covariance between $W1$ and $W2$ bands for N_{ep} (N_{ep}) measurements,

$$C_{12} = \frac{1}{N_{ep} - 1} \sum_i^{N_{ep}} (m[W1]_i - \langle m[W1] \rangle) \times (m[W2]_i - \langle m[W2] \rangle), \quad (3)$$

Σ_{W1} and Σ_{W2} are the standard deviations in $W1$ and $W2$, respectively,

$$\Sigma_{W1} = \sqrt{\frac{1}{N_{ep} - 1} \sum_i^{N_{ep}} (m[W1]_i - \langle m[W1] \rangle)^2}, \quad (4)$$

$$\Sigma_{W2} = \sqrt{\frac{1}{N_{ep} - 1} \sum_i^{N_{ep}} (m[W2]_i - \langle m[W2] \rangle)^2}, \quad (5)$$

where $m[W1]_i$, $m[W2]_i$ are the $W1$, $W2$ magnitudes in the i th epoch, and $\langle m[W1] \rangle$, $\langle m[W2] \rangle$ are the average magnitudes in $W1$, $W2$ respectively, for a given GP source. The amplitude of variability, σ_m is derived as,

$$\sigma_m = \begin{cases} \sqrt{\Sigma^2 - \epsilon^2}, & \text{if } \Sigma > \epsilon \\ 0, & \text{otherwise} \end{cases} \quad (6)$$

where Σ is the photometric variance as defined in equations 4–5, and ϵ is the variance due to measurement errors for N observations in a given band and is defined as,

$$\epsilon^2 = \frac{1}{N} \sum_i^N \epsilon_i^2 + \epsilon_s^2 \quad (7)$$

where ϵ_i is the photometric error of i th epoch, based on the scatter among individual measurements within that epoch, and ϵ_s is the systematic error. For $W1$ and $W2$, the reported systematic uncertainties are 0.024 mag and 0.028 mag, respectively (Jarrett et al. 2011), which are added in quadrature to the photometric uncertainties (ϵ_s in Eqn. 7). Figure 2 shows the distribution of Pearson's correlation coefficient, r , for the GP sample with multi-epoch $WISE$ observations.

True variable objects are those with positive variability amplitudes (σ_{W1} , $\sigma_{W2} > 0$) and strong correlation between $W1$ and $W2$. Sources fulfilling the following criteria were identified as potential AGN candidates: (1) $N_{ep} \geq 5$, (2) σ_1 , $\sigma_2 > 0$, and (3) $r_{12} > 0.6$. The light-curves of these candidate AGN sources were manually inspected to check for anomalies. Some objects showed extreme variability between measurements from the AllWISE and NEOWISE-R epochs; it turns out that there are duplicate extractions of some sources, which fall in the overlap region between two tiles, in the AllWISE observations that are spurious. For those sources, such invalid measurements were excluded and the variability metrics were recomputed. Eventually, a total of 38 GP sources were identified as AGN candidates based on MIR variability. Example light-curves of variable GP sources are shown in Figure 3.

In order to determine the number of false positives in our variable sample, we considered the following. We performed a simple Monte Carlo simulation to calculate the scatter in the Pearson correlation coefficient, r_{12} , assuming a typical non-variable source in our GP sample with median photometric uncertainties in $W1$ and $W2$ bands. Since $N_{ep} \geq 5$ in our variable selection criteria, this simulation was repeated considering light-curves with number of epochs ranging anywhere between 5 to 12 epochs. The number of false positive variable sources in our sample was calculated as follows:

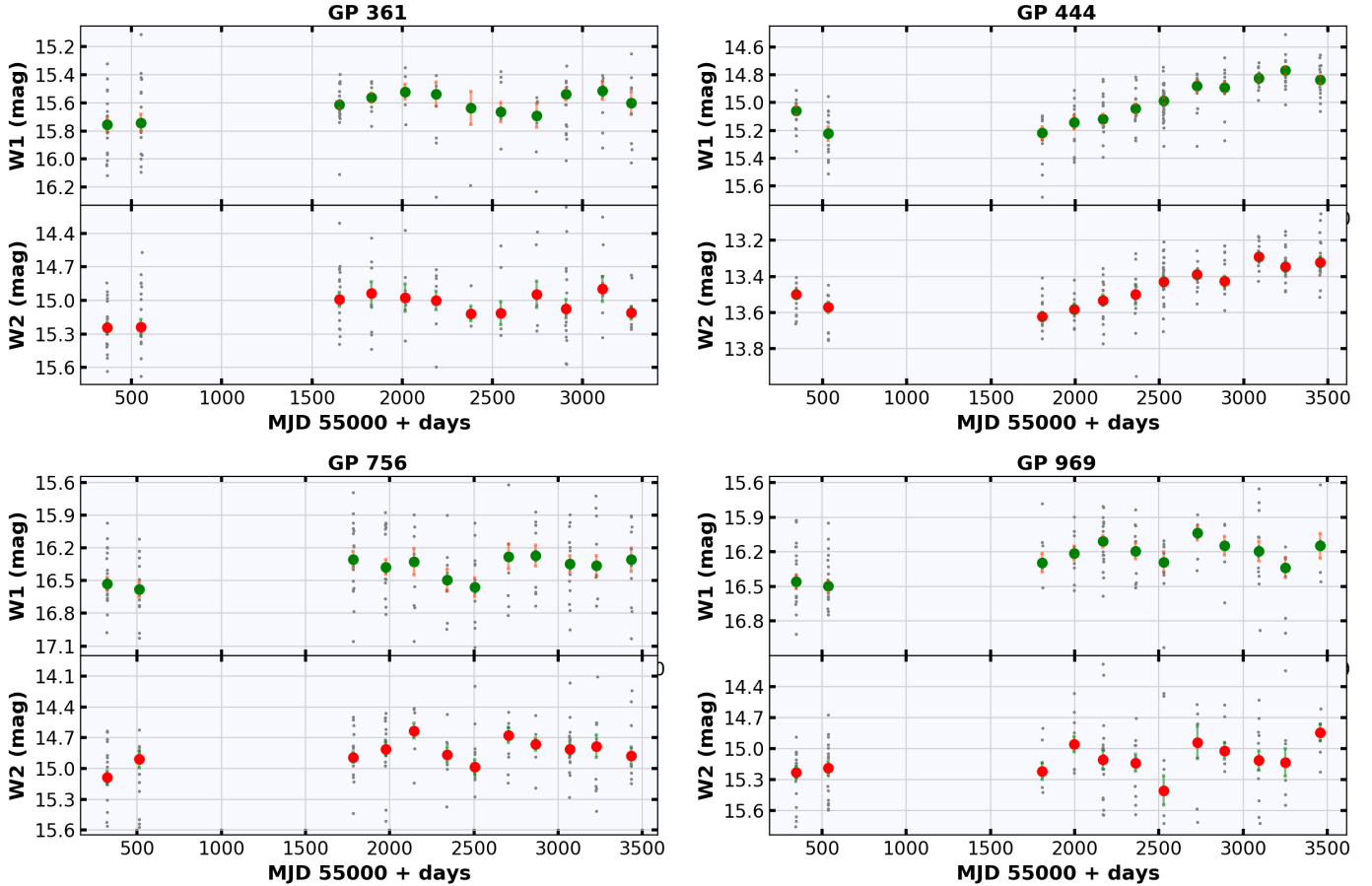


Figure 3. *WISE* light curves in *W1* (top) and *W2* bands (bottom) for four example sources (GP 361, 444, 756, and 969). The magnitudes are based on the Vega system. In each curve, the individual points (red & green) are median values at different epochs (based on single-exposure observations (gray points) within a 30-day epoch) and their respective 1σ Poisson errors. The gap in measurements (between 55600 and 56700 days) corresponds to the time when *WISE* was in hibernation mode.

$$N_{FP} = \sum_{i=5}^{12} N_i \times P(r_{12} > 0.6 : i) \quad (8)$$

where N_i is the number of sources with i epochs in the GP sample and $P(r_{12} > 0.6 : i)$ is the false positive probability for a light-curve with i epochs and Pearson’s $r_{12} > 0.6$. With this method, we found that $N_{FP} \approx 13$ sources could be false positives in our variable sample. A second way to estimate false positives assumes that noise is symmetric. Chance anticorrelations among observed *W1* and *W2* light curves should then be as common as chance positive correlations, while true variable objects should show positive correlations only for plausible variability mechanisms. The number of anticorrelated light curves then serves as a proxy for the number of false positives among the correlated light curves. Based on the distribution of Pearson’s r_{12} for sources with $N_{ep} \geq 5$, we find only 2 sources with $r_{12} < -0.6$ (see Figure 2). Therefore, we conclude that the “real” number of false positives in our variable sample could be anywhere be-

tween 2 and 13 sources, and in any case is only a modest fraction of the 38 detected variables.

4. DISCUSSION

4.1. Limitations of BPT selection

The classical BPT diagram (Baldwin et al. 1981), $\log([\text{NII}]/\text{H}\alpha)$ vs. $\log([\text{OIII}]/\text{H}\beta)$, is a widely employed diagnostic to differentiate AGN from galaxies. Most strong AGN with solar/super-solar metallicity tend to occupy the “rising branch” on the right-hand side of the diagram (Figure 4). However, low metallicity (sub-solar or less) AGN occupy a region on the left-edge of the diagram where they cannot be easily distinguished from star-forming galaxies. Based on chemical evolution estimates from cosmological hydrodynamic simulations, Kewley et al. 2013 showed that low-metallicity galaxies ($12 + \log(\text{O}/\text{H}) \lesssim 8.4$) containing AGN will be impossible to distinguish from low-metallicity star-forming galaxies using the BPT diagram. $\sim 98\%$ of GP objects have metallicities below this limit. Therefore, the BPT dia-

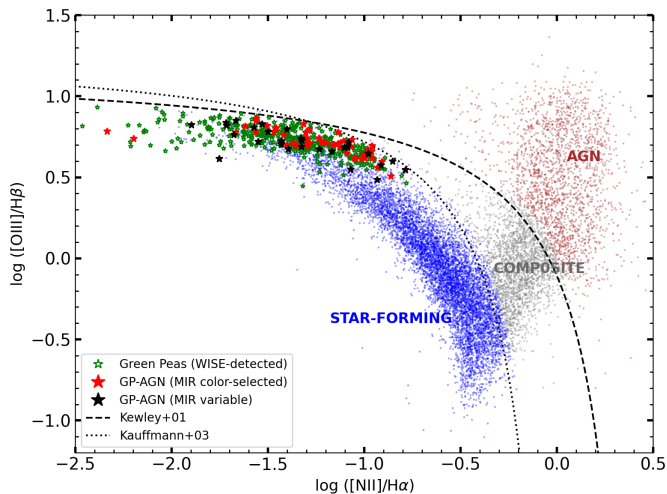


Figure 4. GPs on the BPT diagram. Shown for comparison are SDSS star-forming galaxies (*blue*), composite galaxies (*grey*) and AGN (*red*) from the MPA-JHU catalog. The demarcation lines for star-forming galaxy and AGN populations from Kewley et al. (2001) is represented by *dashed-line* and Kauffmann et al. (2003) is represented by *dotted-line*. GPs selected as AGN based on MIR variability (*black*) and MIR color-color criteria (Jarrett et al. 2011; *red*) are also shown.

gram is inefficient at selecting AGN candidates among the GP sample.

4.2. Nature of MIR color-selected AGN candidates

Different methods of AGN selection can be sensitive to different type of sources with varying luminosities, redshifts, line-of-sight angles, obscuration, and so on. Although X-ray detection is considered to be the most robust diagnostic of AGN presence, a significant fraction of AGN that are selected using infrared diagnostics are not detected in X-rays (e.g., Simmonds et al. 2016). Such sources are expected to be significantly obscured and/or low-luminosity AGN.

MIR color-based selection relies on the fact that hard radiation from an AGN heats the surrounding dusty torus to high temperatures, limited only by the grain sublimation temperature. This produces an approximate power-law continuum in the MIR that is easily distinguishable from stars and typical star-forming galaxies (e.g., Stern et al. 2012; Assef et al. 2013). Since MIR is insensitive to extinction, this selection is able to identify AGN, especially obscured ones that are optically hidden (e.g., Assef et al. 2013; Stern et al. 2014).

Even though red MIR colors are a strong indication of AGN activity in such galaxies, some studies in the past have shown that intense star formation activity in low-metallicity starburst galaxies (such as blue compact dwarfs (BCDs), which are similar to GPs in many ways)

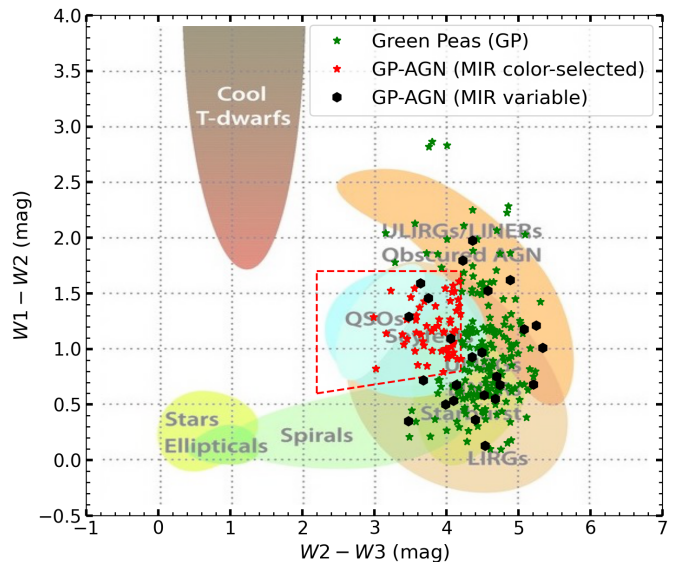


Figure 5. WISE color-color diagram for GP candidate AGN selected based on MIR variability (*black*). For comparison, the color-selected AGN based on Jarrett et al. (2011) criteria are also shown (*red*).

can heat dust to high temperatures that produce extremely red MIR colors (e.g., Griffith et al. 2011; Izotov et al. 2014). Our GP sample has a less extreme typical metallicity ($12+\log(O/H) \sim 8.05$; Jiang et al. 2019), compared to the BCDs in Griffith et al. 2011 ($12+\log(O/H) \sim 7.46$) and Izotov et al. 2014 ($12+\log(O/H) \sim 7.76$), suggesting that GP stellar populations are less likely to produce the observed hot dust emission in the MIR. In fact, our color- and variability-selected AGN candidate sample has a median $12+\log(O/H) \sim 8.17$. Also, according to Satyapal et al. (2018), low-metallicity galaxies with low dust abundance require high column densities, N_H , to produce extreme red WISE colors, while GPs are expected to have low column densities ($N_H \lesssim 10^{20} \text{ cm}^{-2}$; e.g., Yang et al. 2016, 2017b). Also, considering that single-color criteria can suffer from contamination due to star-forming galaxies (e.g., Hainline et al. 2016), we employed the two-color criteria for selection of AGN candidates which is more reliable and robust.

4.3. Comparison of MIR AGN candidates: colors vs. variability

AGN candidates selected based on MIR color selection comprise $\sim 6\%$ of the parent GP sample, whereas candidates based on MIR variability comprise $\sim 4\%$. Only 4 sources (out of 58) that were selected based on MIR colors also exhibited MIR variability in the $W1$ and $W2$ bands of *WISE* (Figure 5). The rest of the variable sample are scattered across the MIR color-color space,

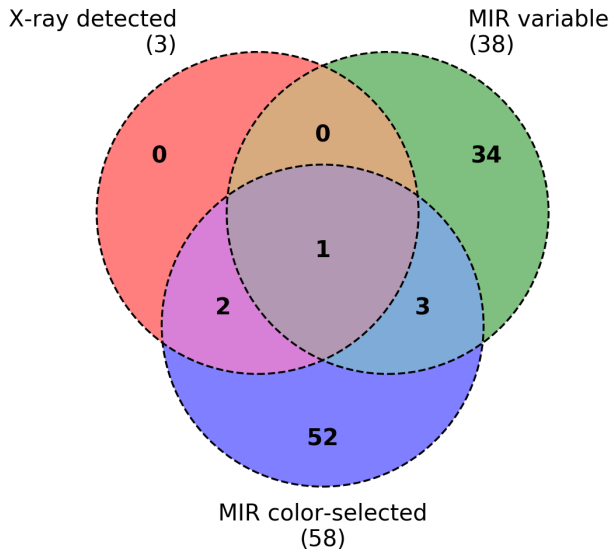


Figure 6. Venn diagram of the AGN samples selected based on MIR colors (*blue*), MIR variability (*green*), and X-ray selection (*red*).

but with typically redder ($W2-W3$) colors. Comparing this with Figure 12 from Wright et al. (2010) which depicts the location of various classes of objects in the WISE color-color space, we find significant number of our variability-selected sources located in regions of the color-color space that is typically inhabited by obscured AGN and LINER (low-ionization nuclear emission-line region) sources (Figure 5). Recently, Polimera et al. (2018) suggested that MIR variability selects a unique population of obscured AGN that could likely be missed by other AGN selection methods, and our findings agree favorably with their observations.

So far, only 3 GPs have published X-ray detections Svoboda et al. (2019); Kawamuro et al. (2019), with X-ray fluxes lower than expected from an AGN but higher than that expected due to extreme star-formation. All three have AGN-like mid-IR colors. Figure 6 shows the overlap of AGN candidates derived based on mid-IR color, mid-IR variability, and known X-ray detections. Based on *XMM-Newton* observations, Svoboda et al. (2019) derive X-ray luminosities ($L_{0.5-8 \text{ keV}}$) for three GPs and find that two of those sources exhibit luminosities 4–6 times larger than expected from the L_X -SFR(-Metallicity) relation. One of those two sources, SDSS J074936.7+333716, is selected as a MIR variable object in the present work. We therefore believe that the measured X-ray excess can be attributed to an obscured AGN in this GP object, in agreement with one of the explanations offered by Svoboda et al. (2019) regarding the X-ray excess.

5. CONCLUSIONS

Using a sample of ~ 1000 GPs selected from SDSS, based on strong $[\text{OIII}]_{\lambda 5007}$ and/or $\text{H}\beta$ emission, we searched for AGN presence in the MIR using *WISE/NEOWISE-R* observations. Our main findings are as follows:

- i. Based on photometry from the shortest three *WISE* bands, we selected a sample of 58 AGN candidates using the color-color criteria from Jarrett et al. (2011).
- ii. For the first time, we used multi-epoch *WISE* observations, spanning a period of 9 years, in the shorter bandpasses ($W1$ and $W2$) to construct light curves for more than 500 GPs. Based on variability amplitude and Pearson’s correlation coefficient (r) metrics, we identified 38 GPs that exhibit notable variability in the MIR, which form a unique sample of AGN candidates, different from the MIR color-selected ones.
- iii. Among MIR color-selected AGN candidates, $\sim 7\%$ of them also exhibit variability in the MIR. In addition, based on archival observations of GPs from *XMM Newton* (Svoboda et al. 2019), 3 of the MIR color-selected AGN have X-ray detections, and at least 2 of these show a significant X-ray excess. One of these is also variable in MIR; therefore, we believe that this excess could be due to accretion activity of an obscured AGN.

Our findings suggest MIR colors and variability can select AGN candidates in low-mass galaxies that elude detection via other selection methods. Since GPs are extreme emission-line galaxies with high specific SFRs and low typical metallicities, optical selection methods may be unable to detect the presence of AGN in GPs, both because optical emission lines may be dominated by star formation activity, and because the optical line ratio signature of AGN becomes less distinct from star formation at low metallicity. Multi-wavelength follow-up observations of these sources will be crucial in validating the AGN presence and constraining their properties, including BH masses and accretion rates. If any of these GPs are shown to not host an AGN, then investigation regarding the origin of hot dust and flux variability will be of great interest in itself.

ACKNOWLEDGMENTS

This publication makes use of data products from the Wide-field Infrared Survey Explorer, which is a joint project of the University of California, Los Angeles, and the Jet Propulsion Laboratory/California Institute of Technology, and NEOWISE, which is a project of the Jet Propulsion Laboratory/California Institute of Technology. WISE and NEOWISE are funded by the National Aeronautics and Space Administration.

Funding for the Sloan Digital Sky Survey IV has been provided by the Alfred P. Sloan Foundation, the U.S. Department of Energy Office of Science, and the Participating Institutions. SDSS-IV acknowledges support and resources from the Center for High Performance Computing at the University of Utah. The SDSS website is www.sdss.org.

SDSS-IV is managed by the Astrophysical Research Consortium for the Participating Institutions of the SDSS Collaboration including the Brazilian Participation Group, the Carnegie Institution for Science, Carnegie Mellon University, Center for Astrophysics — Harvard & Smithsonian, the Chilean Participation Group, the French Participation Group, Instituto de Astrofísica de Canarias, The Johns Hopkins Univer-

sity, Kavli Institute for the Physics and Mathematics of the Universe (IPMU) / University of Tokyo, the Korean Participation Group, Lawrence Berkeley National Laboratory, Leibniz Institut für Astrophysik Potsdam (AIP), Max-Planck-Institut für Astronomie (MPIA Heidelberg), Max-Planck-Institut für Astrophysik (MPA Garching), Max-Planck-Institut für Extraterrestrische Physik (MPE), National Astronomical Observatories of China, New Mexico State University, New York University, University of Notre Dame, Observatório Nacional / MCTI, The Ohio State University, Pennsylvania State University, Shanghai Astronomical Observatory, United Kingdom Participation Group, Universidad Nacional Autónoma de México, University of Arizona, University of Colorado Boulder, University of Oxford, University of Portsmouth, University of Utah, University of Virginia, University of Washington, University of Wisconsin, Vanderbilt University, and Yale University.

This work has made use of the following open-source softwares: SciPy (Virtanen et al. 2020), NumPy (Harris et al. 2020), Matplotlib (Hunter 2007), Astropy (Astropy Collaboration et al. 2013, 2018), DS9 (Joye & Mandel 2003) and TOPCAT (Taylor 2005).

REFERENCES

- Ai, Y. L., Yuan, W., Zhou, H. Y., et al. 2010, *ApJL*, 716, L31, doi: [10.1088/2041-8205/716/1/L31](https://doi.org/10.1088/2041-8205/716/1/L31)
- Aihara, H., Allende Prieto, C., An, D., et al. 2011, *ApJS*, 193, 29, doi: [10.1088/0067-0049/193/2/29](https://doi.org/10.1088/0067-0049/193/2/29)
- Alam, S., Albareti, F. D., Allende Prieto, C., et al. 2015, *ApJS*, 219, 12, doi: [10.1088/0067-0049/219/1/12](https://doi.org/10.1088/0067-0049/219/1/12)
- Assef, R. J., Stern, D., Kochanek, C. S., et al. 2013, *ApJ*, 772, 26, doi: [10.1088/0004-637X/772/1/26](https://doi.org/10.1088/0004-637X/772/1/26)
- Astropy Collaboration, Robitaille, T. P., Tollerud, E. J., et al. 2013, *A&A*, 558, A33, doi: [10.1051/0004-6361/201322068](https://doi.org/10.1051/0004-6361/201322068)
- Astropy Collaboration, Price-Whelan, A. M., Sipőcz, B. M., et al. 2018, *AJ*, 156, 123, doi: [10.3847/1538-3881/aabc4f](https://doi.org/10.3847/1538-3881/aabc4f)
- Baldassare, V. F., Geha, M., & Greene, J. 2018, *ApJ*, 868, 152, doi: [10.3847/1538-4357/aae6cf](https://doi.org/10.3847/1538-4357/aae6cf)
- Baldwin, J. A., Phillips, M. M., & Terlevich, R. 1981, *PASP*, 93, 5, doi: [10.1086/130766](https://doi.org/10.1086/130766)
- Brinchmann, J., Charlot, S., White, S. D. M., et al. 2004, *MNRAS*, 351, 1151, doi: [10.1111/j.1365-2966.2004.07881.x](https://doi.org/10.1111/j.1365-2966.2004.07881.x)
- Cardamone, C., Schawinski, K., Sarzi, M., et al. 2009, *MNRAS*, 399, 1191, doi: [10.1111/j.1365-2966.2009.15383.x](https://doi.org/10.1111/j.1365-2966.2009.15383.x)
- Donley, J. L., Koekemoer, A. M., Brusa, M., et al. 2012, *ApJ*, 748, 142, doi: [10.1088/0004-637X/748/2/142](https://doi.org/10.1088/0004-637X/748/2/142)
- Goulding, A. D., & Alexander, D. M. 2009, *MNRAS*, 398, 1165, doi: [10.1111/j.1365-2966.2009.15194.x](https://doi.org/10.1111/j.1365-2966.2009.15194.x)
- Greene, J. E. 2012, *Nature Communications*, 3, 1304, doi: [10.1038/ncomms2314](https://doi.org/10.1038/ncomms2314)
- Greene, J. E., & Ho, L. C. 2007, *ApJ*, 670, 92, doi: [10.1086/522082](https://doi.org/10.1086/522082)
- Griffith, R. L., Tsai, C.-W., Stern, D., et al. 2011, *ApJL*, 736, L22, doi: [10.1088/2041-8205/736/1/L22](https://doi.org/10.1088/2041-8205/736/1/L22)
- Hainline, K. N., Reines, A. E., Greene, J. E., & Stern, D. 2016, *ApJ*, 832, 119, doi: [10.3847/0004-637X/832/2/119](https://doi.org/10.3847/0004-637X/832/2/119)
- Harris, C. R., Millman, K. J., van der Walt, S. J., et al. 2020, *Nature*, 585, 357–362, doi: [10.1038/s41586-020-2649-2](https://doi.org/10.1038/s41586-020-2649-2)
- Henry, A., Scarlata, C., Martin, C. L., & Erb, D. 2015, *ApJ*, 809, 19, doi: [10.1088/0004-637X/809/1/19](https://doi.org/10.1088/0004-637X/809/1/19)
- Hunter, J. D. 2007, *Computing in science & engineering*, 9, 90
- Izotov, Y. I., Guseva, N. G., Fricke, K. J., & Henkel, C. 2011, *A&A*, 536, L7, doi: [10.1051/0004-6361/201118402](https://doi.org/10.1051/0004-6361/201118402)

- Izotov, Y. I., Guseva, N. G., Fricke, K. J., Krügel, E., & Henkel, C. 2014, *A&A*, 570, A97, doi: [10.1051/0004-6361/201423539](https://doi.org/10.1051/0004-6361/201423539)
- Izotov, Y. I., Schaerer, D., Thuan, T. X., et al. 2016, *MNRAS*, 461, 3683, doi: [10.1093/mnras/stw1205](https://doi.org/10.1093/mnras/stw1205)
- Izotov, Y. I., Worseck, G., Schaerer, D., et al. 2018, *MNRAS*, 478, 4851, doi: [10.1093/mnras/sty1378](https://doi.org/10.1093/mnras/sty1378)
- Jarrett, T. H., Cohen, M., Masci, F., et al. 2011, *ApJ*, 735, 112, doi: [10.1088/0004-637X/735/2/112](https://doi.org/10.1088/0004-637X/735/2/112)
- Jaskot, A. E., & Oey, M. S. 2013, *ApJ*, 766, 91, doi: [10.1088/0004-637X/766/2/91](https://doi.org/10.1088/0004-637X/766/2/91)
- Jiang, T., Malhotra, S., Rhoads, J. E., & Yang, H. 2019, *ApJ*, 872, 145, doi: [10.3847/1538-4357/aee8a](https://doi.org/10.3847/1538-4357/aee8a)
- Joye, W. A., & Mandel, E. 2003, in *Astronomical Society of the Pacific Conference Series*, Vol. 295, *Astronomical Data Analysis Software and Systems XII*, ed. H. E. Payne, R. I. Jedrzejewski, & R. N. Hook, 489
- Kauffmann, G., Heckman, T. M., Tremonti, C., et al. 2003, *MNRAS*, 346, 1055, doi: [10.1111/j.1365-2966.2003.07154.x](https://doi.org/10.1111/j.1365-2966.2003.07154.x)
- Kawamuro, T., Ueda, Y., Ichikawa, K., et al. 2019, *ApJ*, 881, 48, doi: [10.3847/1538-4357/ab2bf6](https://doi.org/10.3847/1538-4357/ab2bf6)
- Kelly, B. C., Bechtold, J., & Siemiginowska, A. 2009, *ApJ*, 698, 895, doi: [10.1088/0004-637X/698/1/895](https://doi.org/10.1088/0004-637X/698/1/895)
- Kewley, L. J., Dopita, M. A., Leitherer, C., et al. 2013, *ApJ*, 774, 100, doi: [10.1088/0004-637X/774/2/100](https://doi.org/10.1088/0004-637X/774/2/100)
- Kewley, L. J., Dopita, M. A., Sutherland, R. S., Heisler, C. A., & Trevena, J. 2001, *ApJ*, 556, 121, doi: [10.1086/321545](https://doi.org/10.1086/321545)
- Kim, K., Malhotra, S., Rhoads, J. E., Butler, N. R., & Yang, H. 2020, *ApJ*, 893, 134, doi: [10.3847/1538-4357/ab7895](https://doi.org/10.3847/1538-4357/ab7895)
- Kim, K. J., Malhotra, S., Rhoads, J. E., & Yang, H. 2021, arXiv e-prints, arXiv:2104.08282, <https://arxiv.org/abs/2104.08282>
- Kormendy, J., & Ho, L. C. 2013, *ARA&A*, 51, 511, doi: [10.1146/annurev-astro-082708-101811](https://doi.org/10.1146/annurev-astro-082708-101811)
- Kormendy, J., & Richstone, D. 1995, *ARA&A*, 33, 581, doi: [10.1146/annurev.aa.33.090195.003053](https://doi.org/10.1146/annurev.aa.33.090195.003053)
- Kozłowski, S., Kochanek, C. S., Ashby, M. L. N., et al. 2016, *ApJ*, 817, 119, doi: [10.3847/0004-637X/817/2/119](https://doi.org/10.3847/0004-637X/817/2/119)
- Kozłowski, S., Kochanek, C. S., Stern, D., et al. 2010, *ApJ*, 716, 530, doi: [10.1088/0004-637X/716/1/530](https://doi.org/10.1088/0004-637X/716/1/530)
- Lacy, M., Petric, A. O., Sajina, A., et al. 2007, *AJ*, 133, 186, doi: [10.1086/509617](https://doi.org/10.1086/509617)
- Lehmer, B. D., Alexander, D. M., Bauer, F. E., et al. 2010, *ApJ*, 724, 559, doi: [10.1088/0004-637X/724/1/559](https://doi.org/10.1088/0004-637X/724/1/559)
- Mainzer, A., Bauer, J., Grav, T., et al. 2011, *ApJ*, 731, 53, doi: [10.1088/0004-637X/731/1/53](https://doi.org/10.1088/0004-637X/731/1/53)
- Maraston, C., Pforr, J., Henriques, B. M., et al. 2013, *MNRAS*, 435, 2764, doi: [10.1093/mnras/stt1424](https://doi.org/10.1093/mnras/stt1424)
- Mateos, S., Alonso-Herrero, A., Carrera, F. J., et al. 2012, *MNRAS*, 426, 3271, doi: [10.1111/j.1365-2966.2012.21843.x](https://doi.org/10.1111/j.1365-2966.2012.21843.x)
- Mineo, S., Gilfanov, M., & Sunyaev, R. 2012, *MNRAS*, 419, 2095, doi: [10.1111/j.1365-2966.2011.19862.x](https://doi.org/10.1111/j.1365-2966.2011.19862.x)
- Nakajima, K., & Ouchi, M. 2014, *MNRAS*, 442, 900, doi: [10.1093/mnras/stu902](https://doi.org/10.1093/mnras/stu902)
- Polimera, M., Sarajedini, V., Ashby, M. L. N., Willner, S. P., & Fazio, G. G. 2018, *MNRAS*, 476, 1111, doi: [10.1093/mnras/sty164](https://doi.org/10.1093/mnras/sty164)
- Reines, A. E., Greene, J. E., & Geha, M. 2013, *ApJ*, 775, 116, doi: [10.1088/0004-637X/775/2/116](https://doi.org/10.1088/0004-637X/775/2/116)
- Ruan, J. J., Anderson, S. F., Dexter, J., & Agol, E. 2014, *ApJ*, 783, 105, doi: [10.1088/0004-637X/783/2/105](https://doi.org/10.1088/0004-637X/783/2/105)
- Satyapal, S., Abel, N. P., & Secrest, N. J. 2018, *ApJ*, 858, 38, doi: [10.3847/1538-4357/aab7f8](https://doi.org/10.3847/1538-4357/aab7f8)
- Sesar, B., Ivezić, Ž., Lupton, R. H., et al. 2007, *AJ*, 134, 2236, doi: [10.1086/521819](https://doi.org/10.1086/521819)
- Simmonds, C., Bauer, F. E., Thuan, T. X., et al. 2016, *A&A*, 596, A64, doi: [10.1051/0004-6361/201629310](https://doi.org/10.1051/0004-6361/201629310)
- Stern, D., Eisenhardt, P., Gorjian, V., et al. 2005, *ApJ*, 631, 163, doi: [10.1086/432523](https://doi.org/10.1086/432523)
- Stern, D., Assef, R. J., Benford, D. J., et al. 2012, *ApJ*, 753, 30, doi: [10.1088/0004-637X/753/1/30](https://doi.org/10.1088/0004-637X/753/1/30)
- Stern, D., Lansbury, G. B., Assef, R. J., et al. 2014, *ApJ*, 794, 102, doi: [10.1088/0004-637X/794/2/102](https://doi.org/10.1088/0004-637X/794/2/102)
- Svoboda, J., Douna, V., Orlitová, I., & Ehle, M. 2019, *ApJ*, 880, 144, doi: [10.3847/1538-4357/ab2b39](https://doi.org/10.3847/1538-4357/ab2b39)
- Taylor, M. B. 2005, in *Astronomical Society of the Pacific Conference Series*, Vol. 347, *Astronomical Data Analysis Software and Systems XIV*, ed. P. Shopbell, M. Britton, & R. Ebert, 29
- Thomas, D., Steele, O., Maraston, C., et al. 2013, *MNRAS*, 431, 1383, doi: [10.1093/mnras/stt261](https://doi.org/10.1093/mnras/stt261)
- Tremonti, C. A., Heckman, T. M., Kauffmann, G., et al. 2004, *ApJ*, 613, 898, doi: [10.1086/423264](https://doi.org/10.1086/423264)
- Trevese, D., Kron, R. G., Majewski, S. R., Bershady, M. A., & Koo, D. C. 1994, *ApJ*, 433, 494, doi: [10.1086/174661](https://doi.org/10.1086/174661)
- Trump, J. R., Sun, M., Zeimann, G. R., et al. 2015, *ApJ*, 811, 26, doi: [10.1088/0004-637X/811/1/26](https://doi.org/10.1088/0004-637X/811/1/26)
- van Wassenhove, S., Volonteri, M., Walker, M. G., & Gair, J. R. 2010, *MNRAS*, 408, 1139, doi: [10.1111/j.1365-2966.2010.17189.x](https://doi.org/10.1111/j.1365-2966.2010.17189.x)
- Virtanen, P., Gommers, R., Oliphant, T. E., et al. 2020, *Nature Methods*, 17, 261, doi: [10.1038/s41592-019-0686-2](https://doi.org/10.1038/s41592-019-0686-2)
- Volonteri, M., & Natarajan, P. 2009, *MNRAS*, 400, 1911, doi: [10.1111/j.1365-2966.2009.15577.x](https://doi.org/10.1111/j.1365-2966.2009.15577.x)

Wright, E. L., Eisenhardt, P. R. M., Mainzer, A. K., et al. 2010, *AJ*, 140, 1868, doi: [10.1088/0004-6256/140/6/1868](https://doi.org/10.1088/0004-6256/140/6/1868)

Yang, H., Malhotra, S., Gronke, M., et al. 2016, *ApJ*, 820, 130, doi: [10.3847/0004-637X/820/2/130](https://doi.org/10.3847/0004-637X/820/2/130)

Yang, H., Malhotra, S., Rhoads, J. E., et al. 2017a, *ApJ*, 838, 4, doi: [10.3847/1538-4357/aa6337](https://doi.org/10.3847/1538-4357/aa6337)

Yang, H., Malhotra, S., Gronke, M., et al. 2017b, *ApJ*, 844, 171, doi: [10.3847/1538-4357/aa7d4d](https://doi.org/10.3847/1538-4357/aa7d4d)